

# A study of events with photoelectric emission in the DarkSide-50 liquid argon Time Projection Chamber

P. Agnes<sup>a</sup>, I. F. M. Albuquerque<sup>b</sup>, T. Alexander<sup>c</sup>, A. K. Alton<sup>d</sup>, M. Ave<sup>b</sup>, H. O. Back<sup>c</sup>, G. Batignani<sup>h,i</sup>, K. Biery<sup>al</sup>, V. Bocci<sup>x</sup>, W. M. Bonivento<sup>j</sup>, B. Bottino<sup>k,l</sup>, S. Bussino<sup>m,n</sup>, M. Cadeddu<sup>j</sup>, M. Cadoni<sup>o,j</sup>, F. Calaprice<sup>ae</sup>, A. Caminata<sup>l</sup>, N. Canci<sup>p</sup>, M. Caravati<sup>j</sup>, N. Cargioli<sup>o,j</sup>, M. Cariello<sup>l</sup>, M. Carlini<sup>p,q</sup>, M. Carpinelli<sup>ar,aj</sup>, S. Catalanotti<sup>s,g</sup>, V. Cataudella<sup>s,g</sup>, P. Cavalcante<sup>ap,p</sup>, S. Cavuoti<sup>s,g,t</sup>, A. Chepurinov<sup>e</sup>, C. Cicalò<sup>j</sup>, A.G. Cocco<sup>g</sup>, G. Covone<sup>s,g</sup>, D. D'Angelo<sup>ao,v</sup>, S. Davini<sup>l</sup>, A. De Candia<sup>s,g</sup>, S. De Cecco<sup>x,y</sup>, G. De Filippis<sup>s,g</sup>, G. De Rosa<sup>s,g</sup>, A. V. Derbin<sup>z</sup>, A. Devoto<sup>o,j</sup>, M. D'Incecco<sup>p</sup>, C. Dionisi<sup>x,y</sup>, F. Dordei<sup>j</sup>, M. Downing<sup>ab</sup>, D. D'Urso<sup>ar,aj</sup>, G. Fiorillo<sup>s,g</sup>, D. Franco<sup>ad</sup>, F. Gabriele<sup>j</sup>, C. Galbiati<sup>ae,p,q</sup>, C. Ghiano<sup>p</sup>, C. Giganti<sup>w</sup>, G. K. Giovanetti<sup>ae</sup>, O. Gorchakov<sup>ah,1</sup>, A.M. Goretti<sup>p</sup>, A. Grobov<sup>aa,ag</sup>, M. Gromov<sup>e,ah</sup>, M. Guan<sup>ai</sup>, Y. Guardincerri<sup>al,1</sup>, M. Gulino<sup>l,aj</sup>, B. R. Hackett<sup>c</sup>, K. Herner<sup>al</sup>, B. Hosseini<sup>j</sup>, F. Hubaut<sup>f</sup>, E.V. Hungerford<sup>a</sup>, An. Ianni<sup>ae,p</sup>, V. Ippolito<sup>x</sup>, K. Keeter<sup>as</sup>, C. L. Kendziora<sup>al</sup>, I. Kochanek<sup>p</sup>, D. Korablev<sup>ah</sup>, G. Korga<sup>a,p</sup>, A. Kubankin<sup>an</sup>, M. Kuss<sup>h</sup>, M. La Commara<sup>s,g</sup>, M. Lai<sup>o,j</sup>, X. Li<sup>ae</sup>, M. Lissia<sup>j</sup>, G. Longo<sup>s,g</sup>, I. N. Machulin<sup>aa,ag</sup>, L. P. Mapelli<sup>aq</sup>, S. M. Mari<sup>m,n</sup>, J. Maricic<sup>af</sup>, C. J. Martoff<sup>am</sup>, A. Messina<sup>x,y</sup>, P. D. Meyers<sup>ae</sup>, R. Milincic<sup>af</sup>, M. Morrocchi<sup>h,i</sup>, V. N. Muratova<sup>z</sup>, P. Musico<sup>l</sup>, A. Navrer Agasson<sup>w</sup>, A.O. Nozdrina<sup>aa,ag</sup>, A. Oleinik<sup>an</sup>, F. Ortica<sup>at,au</sup>, L. Pagani<sup>ac</sup>, M. Pallavicini<sup>k,l</sup>, L. Pandola<sup>aj</sup>, E. Pantic<sup>ac</sup>, E. Paoloni<sup>h,i</sup>, K. Pelczar<sup>p,u</sup>, N. Pelliccia<sup>at,au</sup>, E. Picciau<sup>o,j</sup>, A. Pocar<sup>ab</sup>, S. Pordes<sup>al</sup>, S. S. Poudel<sup>a</sup>, P. Pralavorio<sup>f</sup>, F. Ragusa<sup>ao,v</sup>, M. Razeti<sup>j</sup>, A. Razeto<sup>p</sup>, A. L. Renshaw<sup>a</sup>, M. Rescigno<sup>x</sup>, J. Rode<sup>p,w</sup>, A. Romani<sup>at,au</sup>, D. Sablone<sup>ae,p</sup>, O. Samoylov<sup>ah</sup>, W. Sands<sup>ae</sup>, S. Sanfilippo<sup>n,m</sup>, C. Savarese<sup>q,p,ae</sup>, B. Schlitzer<sup>ac</sup>, D. A. Semenov<sup>z</sup>, A. Shchagin<sup>an</sup>, A. Sheshukov<sup>ah</sup>, M. D. Skorokhvatov<sup>aa,ag</sup>, O. Smirnov<sup>ah</sup>, A. Sotnikov<sup>ah</sup>, S. Stracka<sup>h</sup>, Y. Suvorov<sup>s,g,aa</sup>, R. Tartaglia<sup>p</sup>, G. Testera<sup>l</sup>, A. Tonazzo<sup>ad</sup>, E. V. Unzhakov<sup>z</sup>, A. Vishneva<sup>ah</sup>, R. B. Vogelaar<sup>ap</sup>, M. Wada<sup>ae,j,ak</sup>, H. Wang<sup>aq</sup>, Y. Wang<sup>aq,ai</sup>, S. Westerdale<sup>ae,j</sup>, Ma. M. Wojcik<sup>u</sup>, X. Xiao<sup>aq</sup>, C. Yang<sup>ai</sup>, G. Zuzel<sup>u</sup>

<sup>a</sup>Department of Physics, University of Houston, Houston, TX 77204, USA

<sup>b</sup>Instituto de Física, Universidade de São Paulo, São Paulo 05508-090, Brazil

<sup>c</sup>Pacific Northwest National Laboratory, Richland, WA 99352, USA

<sup>d</sup>Physics Department, Augustana University, Sioux Falls, SD 57197, USA

<sup>e</sup>Skobeltsyn Institute of Nuclear Physics, Lomonosov Moscow State University, Moscow 119234, Russia

<sup>f</sup>Centre de Physique des Particules de Marseille, Aix Marseille Univ, CNRS/IN2P3, CPPM, Marseille, France

<sup>g</sup>INFN Napoli, Napoli 80126, Italy

<sup>h</sup>INFN Pisa, Pisa 56127, Italy

<sup>i</sup>Physics Department, Università degli Studi di Pisa, Pisa 56127, Italy

<sup>j</sup>INFN Cagliari, Cagliari 09042, Italy

<sup>k</sup>Physics Department, Università degli Studi di Genova, Genova 16146, Italy

<sup>l</sup>INFN Genova, Genova 16146, Italy

<sup>m</sup>INFN Roma Tre, Roma 00146, Italy

<sup>n</sup>Mathematics and Physics Department, Università degli Studi Roma Tre, Roma 00146, Italy

<sup>1</sup>Deceased.

- <sup>o</sup>Physics Department, Università degli Studi di Cagliari, Cagliari 09042, Italy  
<sup>p</sup>INFN Laboratori Nazionali del Gran Sasso, Assergi (AQ) 67100, Italy  
<sup>q</sup>Gran Sasso Science Institute, L'Aquila 67100, Italy  
<sup>r</sup>Museo della fisica e Centro studi e Ricerche Enrico Fermi, Roma 00184, Italy  
<sup>s</sup>Physics Department, Università degli Studi "Federico II" di Napoli, Napoli 80126, Italy  
<sup>t</sup>INAF Osservatorio Astronomico di Capodimonte, 80131 Napoli, Italy  
<sup>u</sup>M. Smoluchowski Institute of Physics, Jagiellonian University, 30-348 Krakow, Poland  
<sup>v</sup>INFN Milano, Milano 20133, Italy  
<sup>w</sup>LPNHE, CNRS/IN2P3, Sorbonne Université, Université Paris Diderot, Paris 75252, France  
<sup>x</sup>INFN Sezione di Roma, Roma 00185, Italy  
<sup>y</sup>Physics Department, Sapienza Università di Roma, Roma 00185, Italy  
<sup>z</sup>Saint Petersburg Nuclear Physics Institute, Gatchina 188350, Russia  
<sup>aa</sup>National Research Centre Kurchatov Institute, Moscow 123182, Russia  
<sup>ab</sup>Amherst Center for Fundamental Interactions and Physics Department, University of Massachusetts, Amherst, MA 01003, USA  
<sup>ac</sup>Department of Physics, University of California, Davis, CA 95616, USA  
<sup>ad</sup>APC, Université de Paris, CNRS, Astroparticule et Cosmologie, Paris F-75013, France  
<sup>ae</sup>Physics Department, Princeton University, Princeton, NJ 08544, USA  
<sup>af</sup>Department of Physics and Astronomy, University of Hawai'i, Honolulu, HI 96822, USA  
<sup>ag</sup>National Research Nuclear University MEPhI, Moscow 115409, Russia  
<sup>ah</sup>Joint Institute for Nuclear Research, Dubna 141980, Russia  
<sup>ai</sup>Institute of High Energy Physics, Beijing 100049, China  
<sup>aj</sup>INFN Laboratori Nazionali del Sud, Catania 95123, Italy  
<sup>ak</sup>AstroCeNT, Nicolaus Copernicus Astronomical Center, 00-614 Warsaw, Poland  
<sup>al</sup>Fermi National Accelerator Laboratory, Batavia, IL 60510, USA  
<sup>am</sup>Physics Department, Temple University, Philadelphia, PA 19122, USA  
<sup>an</sup>Radiation Physics Laboratory, Belgorod National Research University, Belgorod 308007, Russia  
<sup>ao</sup>Physics Department, Università degli Studi di Milano, Milano 20133, Italy  
<sup>ap</sup>Virginia Tech, Blacksburg, VA 24061, USA  
<sup>aq</sup>Physics and Astronomy Department, University of California, Los Angeles, CA 90095, USA  
<sup>ar</sup>Chemistry and Pharmacy Department, Università degli Studi di Sassari, Sassari 07100, Italy  
<sup>as</sup>School of Natural Sciences, Black Hills State University, Spearfish, SD 57799, USA  
<sup>at</sup>INFN Perugia, Perugia 06123, Italy  
<sup>au</sup>Chemistry, Biology and Biotechnology Department, Università degli Studi di Perugia, Perugia 06123, Italy

---

## Abstract

Finding unequivocal evidence of dark matter interactions in a particle detector is a major objective of physics research. Liquid argon time projection chambers offer a path to probe Weakly Interacting Massive Particles scattering cross sections on nucleus down to the so-called neutrino floor, in a mass range from few GeV's to hundredths of TeV's. Based on the successful operation of the DarkSide-50 detector at LNGS, a new and more sensitive experiment, DarkSide-20k, has been designed and is now under construction. A thorough understanding of the DarkSide-50 detector response and, therefore, of all kind of observed events, is essential for an optimal design of the new experiment. In this paper, we report on a particular set of events, which were not used for dark matter searches. Namely, standard two-pulse scintillation-ionization signals accompanied by a small amplitude third pulse, originating from single or few electrons, in a time window of less than a maximum drift time. We

compare our findings to those of a recent paper of the LUX Collaboration (D.S.Akerib et al. Phys.Rev.D 102, 092004). Indeed, both experiments observe events related to photoionization of the cathode. From the measured rate of these events, we estimate for the first time the quantum efficiency of the tetraphenyl butadiene deposited on the DarkSide-50 cathode at wavelengths around 128 nm, in liquid argon. Also, both experiments observe events likely related to photoionization of impurities in the liquid. The probability of photoelectron emission per unit length turns out to be one order of magnitude smaller in DarkSide-50 than in LUX. This result, together with the much larger measured electron lifetime, coherently hints toward a lower concentration of contaminants in DarkSide-50 than in LUX.

*Keywords:* Dark matter, liquid argon, underground argon

---

## 1. Introduction

Direct detection of Weakly Interacting Massive Particle Dark Matter (WIMP DM) is one of the most active areas of astroparticle physics. The Liquid Argon (LAr) Time Projection Chamber (TPC) technology offers a path to reach sensitivities to WIMP-nucleus scattering cross-sections down to the so-called neutrino floor [1], for both high and low WIMP masses.

Based on the successful operation of the DarkSide-50 (DS-50) detector [2, 3], a larger and more sensitive experiment, DarkSide-20k (DS-20k) [4], is now under construction. A deep understanding of the DS-50 detector response is one of key ingredients for an optimal design of DS-20k. Therefore, beyond studying events related to dark matter searches, it is very important to scrutinize all event types in the detector, since they may provide hints for detector optimization.

A typical interaction in the active volume of the TPC yields a prompt scintillation signal, S1, and one or more clouds of ionization electrons, depending on the single- or multi-scatter nature of the interaction. In the DS-50 LAr TPC, ionization electrons drift upwards under a uniform electric field and are, under the application of two other fields, extracted into the gas pocket and induce one or more electroluminescence sig-

nals, S2. As discussed in [5], S1 and S2 signals have different pulse shapes. The S1 signal rises in few ns and falls as a double exponential, with  $\tau_1 = (6 \pm 1)$  ns and  $\tau_2 = (1.5 \pm 0.1)$   $\mu$ s, and an amplitude ratio of the two exponentials of  $\sim 3$  for nuclear recoils and  $\sim 0.3$  for electron recoils [6, 7]. This difference in amplitude ratios leads to a very effective Pulse Shape Discrimination (PSD) between electron and nuclear recoils. The S2 signal has a different pulse shape, i.e. a  $\sim 1$   $\mu$ s rise-time and a  $\sim 3$   $\mu$ s fall-time. The detection of both S1 and S2 pulses allows three-dimensional reconstruction of the interaction point and, therefore, background rejection by detection of multiple interactions and volume fiducialization. In DS-50 the typical pulse charge ratio S2 over S1, as discussed in section 2, is between 10 and 30. Therefore, low energy interactions may yield only S2 signals above detection threshold. These single-pulse events were exploited to extend dark matter searches to lower masses [2].

In addition to these *standard* events, other event types were observed in the DS-50 detector. In this paper, we discuss *prompt* emission events, namely events with an additional small amplitude S2 pulse, referred to as Single Electron Candidate (SEC) in the following, occurring in the same 440  $\mu$ s data acquisition window of standard events. We classify these events

into two different categories: *echo events*, discussed in section 4, when the SEC has a definite temporal relationship with the preceding S1 or S2, and *bulk events*, discussed in section 5, when the SEC does not have a definite temporal relationship with the preceding S1 or S2, but it is consistent with being due to one single electron. Therefore, both these event types have features that clearly distinguish them from the trivial multi-scatter photon background interactions.

Events with single electron signals occurring outside of the acquisition window of a previous standard event, i.e. due to a *delayed* emissions, were also observed in DS-50 [2] and will be further discussed and analyzed in an upcoming DS-50 publication.

Based on the study detailed in this paper, we also provide an interpretation of observed event types.

Similar kinds of events as those discussed in this paper were also observed and studied with xenon detectors. The most comprehensive study was performed by the LUX Collaboration [8] and we will use it for comparison with our results. Other previous papers reporting similar event types can be found in Refs. [9, 10, 11].

## 2. The DarkSide-50 detector

The DS-50 LAr TPC detects light from both S1 and S2 using 38 3" photomultipliers (PMTs) arranged in two arrays of 19 PMTs each, at both ends of the  $(46.4 \pm 0.7)$  kg cylindrical active target of low-radioactivity underground argon (UAr) [12, 13, 14]. The PMTs are submerged in liquid argon and view the active volume through fused silica windows. These are coated on both faces with transparent conductive indium tin oxide (ITO) films 15 nm thick. The inner window faces define the grounded anode (top) and HV cathode

(bottom) of the TPC, while the outer faces are kept at the average photocathode potential of each 19-PMT array. The cylindrical side wall is made of 2.54 cm-thick polytetrafluoroethylene (PTFE) reflector sintered using a special annealing cycle to increase its reflectivity. The PTFE reflector and the fused silica windows are coated with tetraphenyl butadiene (TPB) wavelength shifter, which absorbs the 128 nm LAr scintillation photons and re-emits visible photons with a peak wavelength of 420 nm. The specific thickness of the TPB coating on the windows varies between  $(230 \pm 10) \mu\text{g}/\text{cm}^2$  at the center and  $(190 \pm 15) \mu\text{g}/\text{cm}^2$  at the edge of the active volume, corresponding to few  $\mu\text{m}$  thickness. The thickness of the TPB on the cylindrical wall is  $(165 \pm 20) \mu\text{g}/\text{cm}^2$  at half-height and  $(224 \pm 27) \mu\text{g}/\text{cm}^2$  at the top and bottom. The electric fields needed for drifting and extracting electrons consists of the ITO-coated cathode and anode planes, a field cage comprising a stack of copper rings behind the PTFE reflector held at graded potentials, and a grid that separates the drift and electron extraction regions. The grid, placed 5 mm below the liquid surface, is a hexagonal mesh photo-etched from a 50  $\mu\text{m}$ -thick stainless steel foil and has an optical transparency of 95% at normal incidence.

The data reported in this paper were acquired between July 2015 and October 2017, using a TPC drift field of 200 V/cm, an extraction field of 2.8 kV/cm, and an electroluminescence field of 4.2 kV/cm. At this extraction field, the efficiency for extracting ionization electrons into the gas layer is estimated to be close to 100% [15, 16]. The electron drift time,  $t_{\text{drift}} = \Delta t_{\text{S2-S1}}$ , has a maximum value at  $t_{\text{drift}}^{\text{max}} = 376 \mu\text{s}$ , for interactions located right above the cathode. The electron drift speed is  $(0.93 \pm 0.01) \text{ mm}/\mu\text{s}$  [17].

A hardware trigger in DS-50 occurs when

two or more PMT signals exceed a threshold of 0.6 Photo-Electrons (PE) within a 100 ns window. Waveform data are recorded from all 38 PMTs for 440  $\mu\text{s}$  starting  $\sim 10 \mu\text{s}$  before the trigger. Subsequent triggers are inhibited for 810  $\mu\text{s}$ . Software pulse-finding algorithms are then applied to the digitized data, including the pre-trigger data. The software classifies the pulses into two categories (S1 or S2) based on the fraction of light detected within the first 90 ns ( $f_{90}$ ). The efficiency of the software pulse-finding algorithm is essentially 100% for S2 signals larger than 30 PE [18]. The pulse finder uses an integration window of 30  $\mu\text{s}$ , which is long enough to include the entire S2 signal.

The argon is purified continuously by recirculating it in gaseous form through a heated getter (SAES Monotorr PS4-MT50-R-2), which reduces contaminants such as  $\text{O}_2$  and  $\text{N}_2$  to sub-ppb levels, and through a cold charcoal radon trap. The measured electron lifetime was larger than  $\sim 8$  ms during the whole data-taking, corresponding to  $\sim 35$  ppt  $\text{O}_2$ -equivalent contamination [19].

### 3. Event selection

We select three-pulse events, with an S1 followed by two S2. The S1 pulse provides the event trigger. One of the S2 pulses, the SEC, is required to have a charge smaller than 200 PE.

We require the event trigger to occur at least 400  $\mu\text{s}$  after the end of the inhibit window of the previous trigger, namely at least 1.21 ms after the previous trigger. This removes events which triggered on an S2, with the corresponding S1 occurring during the inhibit window [12].

The S2 light yield drops by about 60% from the center to the sides of the detector [20]. To avoid efficiency corrections, we only select events with the maximum of the

SEC signal in the central top PMT. The corresponding effective surface cathode area is a circle of about 9 cm diameter. Moreover, to simplify efficiency calculations, we select events with the maximum of the S2 signal in one of the 19 top PMTs.

The trigger, as shown in Ref.[2], is fully efficient for pulses above 30 PE, and, since all events studied here are triggered by S1, the trigger inefficiency is completely negligible.

The  $f_{90}$  variable is also used to distinguish between electron and nuclear recoils. Indeed, for electron recoils its value clusters around 0.3 while for nuclear recoils around 0.7. For the rest of this paper, we restrict our selection to electron recoil events, by requiring  $f_{90} < 0.5$ . Moreover, to limit saturation effects and pulse overlaps we require  $\text{S2} < 50,000$  PE and  $100 \text{ PE} < \text{S1} < 1500$  PE.

We classify the selected events into two groups, according to the time sequence of the three pulses: S1-S2-SEC, with the SEC occurring after the S2 pulse, and S1-SEC-S2, with the SEC occurring between S1 and S2.

To further strengthen the correct identification of the pulse sequence, we require the ratio of S2 to S1 to be larger than 10, as expected when the two pulses come from the same electron recoil interaction. Indeed, in DS-50, the typical S2 to S1 charge ratio for electron recoils is between 10 and 30.

### 4. Echo events

For S1-S2-SEC events, figure 1 shows the charge of the SEC pulse vs. the time difference,  $\Delta t_{\text{SEC-S2}}$ , between the SEC and the preceding S2. We observe three main features in the plot, corresponding to three sets of events, which will be detailed in the following sections.

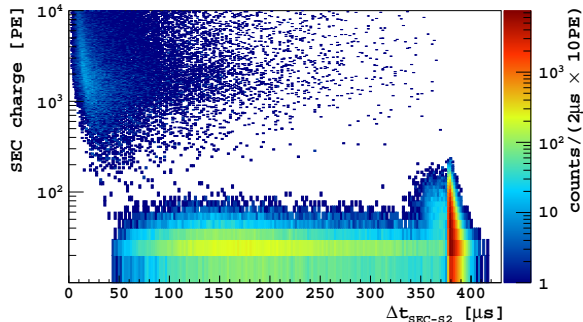


Figure 1: SEC charge vs. time difference between the SEC and the preceding S2 pulse,  $\Delta t_{\text{SEC-S2}}$ . The set of events at small values of  $\Delta t_{\text{SEC-S2}}$  and large values of charge is related to double-scatter  $\gamma$ -ray interactions.

#### 4.1. S2-echo events

One set of events in figure 1 is clustered around  $\Delta t_{\text{SEC-S2}} \sim 380 \mu\text{s}$ , corresponding to about the maximum TPC drift time, and SEC charges extending up to a few hundred PEs. It seems plausible that these events are due to S2 photons extracting electrons from the cathode. The electrons then drift under the electric field through the whole TPC length. Moreover, the S2 pulses are quite large signals and, sometimes, more than one photon is able to induce electron emission from the cathode. We call these events *S2-echo* events. Figure 2 shows the SEC charge spectrum for these events. The peak corresponding to one electron is visible and its corresponding SEC charge is in agreement with the observation of a previous DS-50 paper [2] of  $\sim 23$  PE. Also, the distribution shows a tail extending to few electron signal.

The number of S2-echo events recorded on disk is affected by the data acquisition time window of  $430 \mu\text{s}$  after the trigger. This time window is smaller than  $2t_{\text{drift}}^{\text{max}}$ , the time that would be required for recording all S2-echo events. Indeed, when requiring three-pulse events, the DS-50 data acquisition only record S2-echo events originating from interactions in the top section of

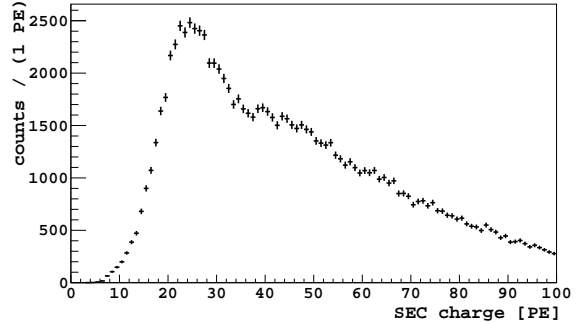


Figure 2: SEC charge spectrum for S2-echo events.

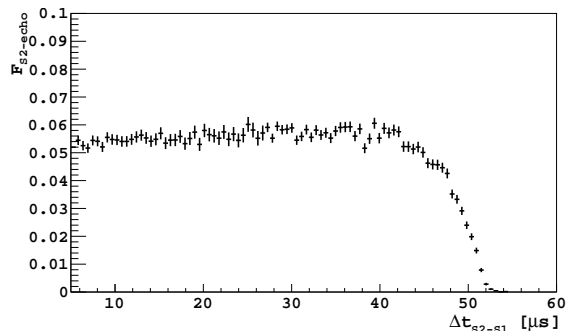


Figure 3: Fraction of events with an S2-echo, as a function of the drift time,  $\Delta t_{\text{S2-S1}}$ .

the TPC, with S1-S2 drift times,  $\Delta t_{\text{S2-S1}}$ , smaller than  $430 \mu\text{s} - t_{\text{drift}}^{\text{max}} \sim 50 \mu\text{s}$ . Figure 3 shows the fraction of events containing an S2-echo, as a function of the drift time, i.e.:

$$F_{\text{S2-echo}}(t_{\text{drift}}) = N_{\text{S2-echo}}(t_{\text{drift}}) / N_{\text{S2}}(t_{\text{drift}}). \quad (1)$$

The drift time,  $\Delta t_{\text{S2-S1}}$ , is of course a measurement of the depth of the interaction,  $z$ , with  $z = 0$  corresponding to  $\Delta t_{\text{S2-S1}} = 0$ , i.e. the gas-liquid interface.

If our interpretation of the S2-echo events were correct, we should expect that, the larger the S2 charge, the larger the probability of inducing photoelectric emission from the cathode of more than one electron. Indeed this is observed in figure 4, which shows the SEC charge vs. S2 charge distribution, for S2-echo events. Overlaid is the profile histogram, which clearly shows the expected correlation.

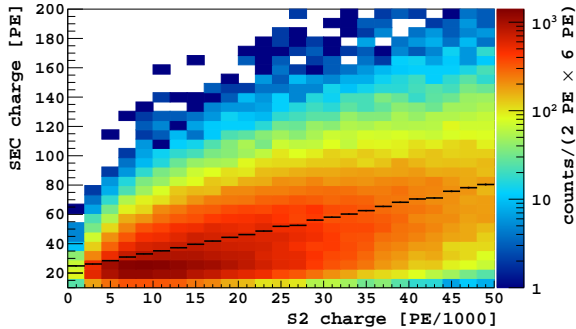


Figure 4: SEC charge vs. S2 charge distribution for S2-echo events. Overlaid is the profile histogram. A linear fit gives an intercept of  $\sim 23.3$  PE and a slope of  $\sim 1.2 \times 10^{-3}$ .

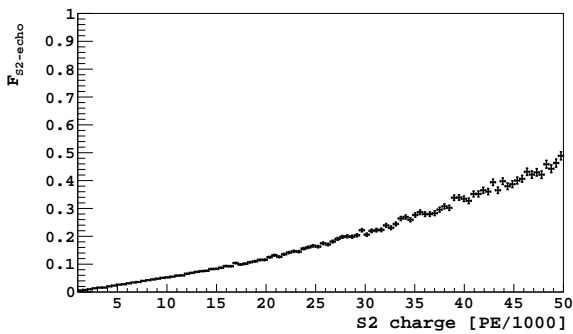


Figure 5: Fraction of events containing S2-echoes vs. S2 charge, with  $5\mu\text{s} < \Delta t_{\text{S2-S1}} < 45\mu\text{s}$ .

We also expect that the probability of S2-echo events, regardless of the SEC pulse charge, increases with the S2 pulse charge. Indeed, this is what is observed in figure 5, which shows the fraction of events with an S2-echo as a function of the S2 charge. This fraction is found to monotonically increase with the S2 charge, leading to an event fraction of about 0.5 at the maximum S2 selected energy.

Therefore, S2-echo events, taking into account that we only select events in the central top PMT out of 19, are very frequent. Indeed, they are present in almost every event, though in DS-50 data, due to the limited data acquisition time window, most of the third pulses are not recorded on disk.

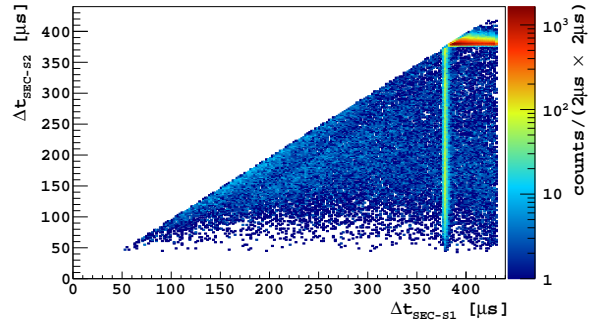


Figure 6: Time difference  $\Delta t_{\text{SEC-S2}}$  vs. time difference  $\Delta t_{\text{SEC-S1}}$  distribution for events with  $\text{SEC} < 50$  PE.

#### 4.2. S1-echo events

Another set of events in figure 1 is clustered at  $\Delta t_{\text{SEC-S2}}$  between  $50\mu\text{s}$  and  $375\mu\text{s}$  and SEC charges peaking at  $\sim 25$  PE, corresponding to the single-electron response. These events are well separated from those at SEC charges larger than a few 100 PEs, that are instead identified as S2 events from standard double-scatter  $\gamma$ -ray interactions in the detector. It can be noticed that, the pulse finder is not able to reconstruct SEC pulses below  $\sim 100$  PE that are less than  $\sim 40\mu\text{s}$  apart from an S2 pulse.

The origin of these events can be understood from figure 6, which shows the distribution of  $\Delta t_{\text{SEC-S2}}$  vs.  $\Delta t_{\text{SEC-S1}}$ , when selecting events with  $\text{SEC} < 50$  PE.

Three event categories are clearly visible in the distribution: a horizontal band at  $\Delta t_{\text{SEC-S2}} \sim 380\mu\text{s}$ , corresponding to the S2-echo events discussed in section 4.1, a continuum of events without a specific time relation of the SEC with either S1 or S2, which will be discussed in section 5, and a vertical band, corresponding to  $\Delta t_{\text{SEC-S1}} \sim 380\mu\text{s}$ , about one maximum drift time after the S1 signal. We interpret these events, for  $\Delta t_{\text{SEC-S2}} < 375\mu\text{s}$ , as photoelectric emissions from the cathode induced by S1 photons and call them *S1-echo* events. The narrowness of the time distribution of the S1-echo events, shown in figure 7, which dis-

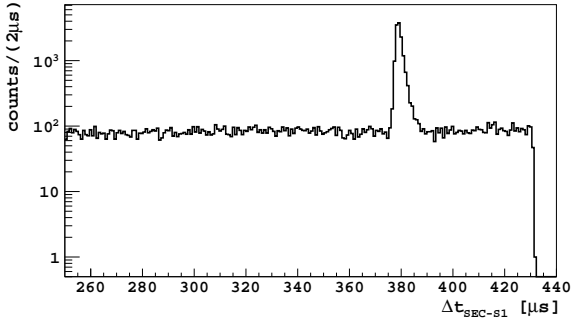


Figure 7: Time difference  $\Delta t_{\text{SEC-S1}}$  distribution, for events with  $\text{SEC} < 50$  PE and  $\Delta t_{\text{SEC-S2}} < 350$   $\mu\text{s}$ .

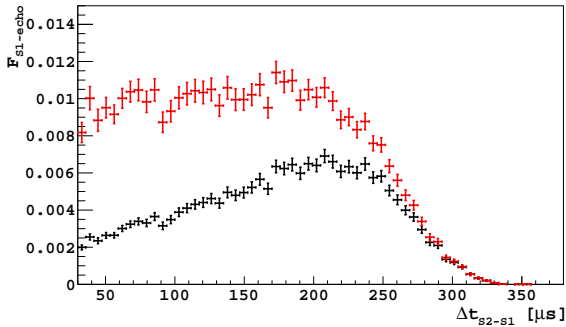


Figure 8: Fraction of events with an S1-echo,  $F_{\text{S1-echo}}$ , vs. drift time  $\Delta t_{\text{S2-S1}}$  (black dots) and after efficiency corrections (red dots),  $F_{\text{S1-echo}}^\epsilon$ , scaled by a factor 0.01.

plays  $\Delta t_{\text{SEC-S1}}$  for events with  $\text{SEC} < 50$  PE and  $\Delta t_{\text{SEC-S2}} < 350$   $\mu\text{s}$ , also confirms the expectation that, since the electron extraction efficiency in the gas pocket is close to 100%, substantial delayed emission from the liquid surface on the scale of 10 to 100  $\mu\text{s}$  is excluded.

Figure 8 shows the fraction of events with an S1-echo,  $F_{\text{S1-echo}}$ , vs. the drift time,  $\Delta t_{\text{S2-S1}}$ , defined as:

$$F_{\text{S1-echo}}(t_{\text{drift}}) = \frac{N_{\text{S1-echo}}(t_{\text{drift}})}{N_{\text{S2}}(t_{\text{drift}})}, \quad (2)$$

with  $N_{\text{S2}}(t_{\text{drift}})$  the selected total number of events (two pulse and three pulse).  $F_{\text{S1-echo}}$  rises up to about 250  $\mu\text{s}$ , due to acceptance effects, whereas it drops at large  $\Delta t_{\text{S2-S1}}$ , when the time of the SEC become closer to

the preceding S2. This drop is due to a pulse finder inefficiency, likely the same effect seen in figure 1, which tends to merge small signals with a preceding S2. Indeed, when for instance we select low energy events, such as with  $\text{S1} < 800$  PE and  $\text{S2} < 5000$  PE, we find that the drop at large  $\Delta t_{\text{S2-S1}}$  only starts at  $\sim 300$   $\mu\text{s}$ . As a matter of fact, no tuning of the pulse finder algorithm was ever made to cope with this effect. We also tested the hypothesis that the drop could be due to the SEC being captured by the ion cloud of the S2 signal, by selecting events for which the S2 signal maximum is not in the central PMT. The corresponding distribution of figure 8 does not change and, therefore, we discard this hypothesis. The presence of a time gap between the S2 and the subsequent SEC is also visible in the continuum of events at the bottom of figure 6.

The efficiency for S1-echo events,  $\epsilon(r, t_{\text{drift}})$ , was calculated with a toy Monte Carlo as the fraction of S1 UV photons, for which we assume  $4\pi$  emission at given  $r$  and  $z$  position in the chamber corresponding to a given  $t_{\text{drift}}$ , that hit a cathode area corresponding to the central PMT. In the following, we made the simplifying assumption, true to a good approximation, that the event distribution in  $t_{\text{drift}}$  and  $r$  factorize. Then, the average  $\hat{\epsilon}(t_{\text{drift}})$  is obtained by weighting the efficiency  $\epsilon(r, t_{\text{drift}})$  by the radial distribution,  $f(r)$ , of the S2 pulses measured with data, as:

$$\hat{\epsilon}(t_{\text{drift}}) = \sum_r \epsilon(r, t_{\text{drift}}) f(r), \quad (3)$$

The radial distribution of S2 events is shown in figure 9 and is peaked at large  $r$  due to the material radioactivity. For  $t_{\text{drift}} < 330$   $\mu\text{s}$ , the calculated efficiency is a rising function of  $t_{\text{drift}}$  and can be parametrized as:

$$\hat{\epsilon}(t_{\text{drift}}) = 0.0072 \cdot e^{0.0024 \cdot t_{\text{drift}}} - 0.0054. \quad (4)$$

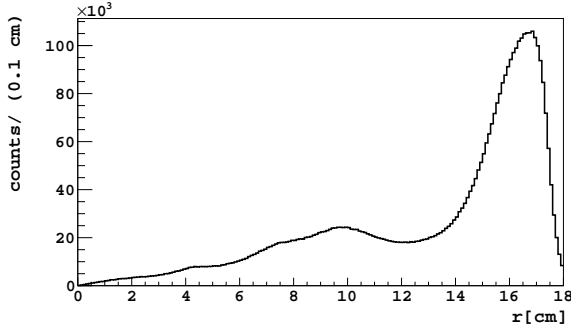


Figure 9: Radial distribution of S2 pulses for events with  $\Delta t_{S2-S1} > 50 \mu s$ .

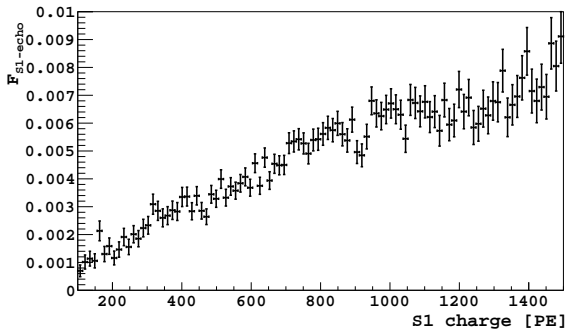


Figure 10: Fraction of events with an S1-echo vs. S1 charge, with  $50 \mu s < \Delta t_{S2-S1} < 200 \mu s$ .

The fraction of events with an S1-echo vs. drift time, after efficiency corrections, defined as

$$F_{S1-echo}^{\epsilon}(t_{\text{drift}}) = \frac{N_{S1-echo}(t_{\text{drift}})}{\hat{\epsilon}(t_{\text{drift}})N_{S2}(t_{\text{drift}})}, \quad (5)$$

is shown in red in Figure 8. Below  $\sim 200 \mu s$  we retrieve a flat distribution (the value of  $F_{S1-echo}^{\epsilon}$  may go above one since we consider UV-photon emission in  $4\pi$ ).

By analogy with figure 5, we show in figure 10 the fraction of events containing S1-echoes vs. S1 charge, with  $50 \mu s < \Delta t_{S2-S1} < 200 \mu s$ . Again larger S1 pulses have larger probability to produce also S1-echoes. Figure 11 shows the SEC charge distribution for selected S1-echo events. The peak corresponding to one extracted electron can be clearly observed. A shoulder due to two extracted electrons can also be noticed.

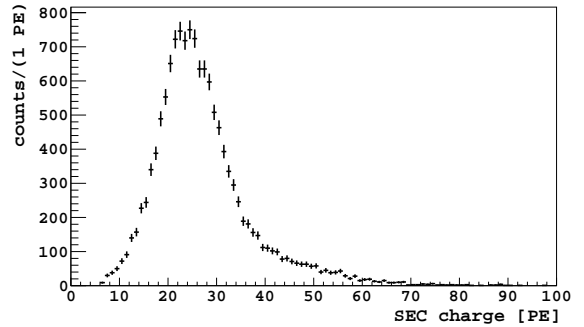


Figure 11: SEC charge spectrum for S1-echo events.

#### 4.3. Calculation of the cathode quantum efficiency

From the measured fraction of both S1-echo and S2-echo events it is possible to estimate the quantum efficiency of the cathode in liquid argon,  $QE$ , i.e the photoelectron emission probability per UV photon,  $\gamma_{UV}$ , at the liquid argon emission wavelengths of  $\sim 128 \text{ nm}$ .

We select events with  $50 \mu s < \Delta t_{S2-S1} < 200 \mu s$ . Indeed, we showed in section 4.2 that for these drift times we understand our efficiency corrections as we are able to retrieve a flat distribution as a function of  $t_{\text{drift}}$ . Then:

$$N_{S1-echo}(t_{\text{drift}}) = \hat{\epsilon}(t_{\text{drift}})N_{\gamma_{UV}}(t_{\text{drift}})QE_{S1}, \quad (6)$$

where the number of UV photons is given by:

$$N_{\gamma_{UV}}(t_{\text{drift}}) = N_{S2}(t_{\text{drift}})\langle S1 \rangle / g_1. \quad (7)$$

with  $g_1 \sim 0.16 \text{ PE}/\gamma_{UV}$  [20] the collection efficiency of S1 photons generated in liquid argon, and  $\langle S1 \rangle$  the S1 mean charge expressed in PE and assumed to be independent of  $r$  and  $t_{\text{drift}}$ .

Since in the selected  $\Delta t_{S2-S1}$  range  $F_{S1-echo}^{\epsilon}$  turns out to be about constant (see figure 8),  $\langle F_{S1-echo}^{\epsilon} \rangle \sim 1.0$ , combining eq. (5), eq. (6), and eq. (7), we obtain

$$QE_{S1} \sim \langle F_{S1-echo}^{\epsilon} \rangle \frac{g_1}{\langle S1 \rangle} \quad (8)$$

Since  $\langle S1 \rangle \sim 730$  PE, we obtain  $QE_{S1} \sim 3 \times 10^{-4}/\gamma_{UV}$ .

The S2-echo photons are induced by S2 signals. Therefore, only one value for average geometric efficiency is needed,  $\hat{\epsilon}_{S2}$ , which corresponds to the value calculated from eq. (4) at  $t_{\text{drift}} \sim 0$ . The number of events with S2-echo is given by:

$$N_{S2\text{-echo}}(t_{\text{drift}}) = \hat{\epsilon}_{S2} N_{S2}(t_{\text{drift}}) \frac{\langle S2 \rangle}{\langle N_{el} \rangle g_2} QE_{S2}, \quad (9)$$

where  $\langle N_{el} \rangle$  is the average number of electrons per S2-echo event and  $g_2 \sim 0.16$  PE/ $\gamma_{UV}$  [20, 21]. Since

$$\langle N_{el} \rangle = \langle \text{SEC} \rangle / g \quad (10)$$

with  $\langle \text{SEC} \rangle$  the average SEC charge in PE and  $g \sim 23$  PE/ $e^-$  the photoelectric gain in the central PMT. Defining  $K = g/g_2$  and taking the average of  $F_{S2\text{-echo}}$ , defined in eq. (1), over the interval  $5 \mu\text{s} < \Delta t_{S2-S1} < 45 \mu\text{s}$ , we obtain:

$$QE_{S2} \sim \langle F_{S2\text{-echo}} \rangle \frac{1}{K \hat{\epsilon}_{S2}} \frac{\langle \text{SEC} \rangle}{\langle S2 \rangle} \quad (11)$$

Now, from figure 3 we derive  $\langle F_{S2\text{-echo}} \rangle \sim 0.055$ , and we have  $\langle \text{SEC} \rangle \sim 49$  PE,  $\langle S2 \rangle \sim 23,430$  PE and  $\hat{\epsilon}_{S2} \sim 3 \cdot 10^{-3}$ . Eventually, we obtain  $QE_{S2} \sim 4 \times 10^{-4}/\gamma_{UV}$ .

Both  $QE_{S1}$  and  $QE_{S2}$  measurements, in fair agreement with each other, are affected by systematic uncertainties due to the dependence of both  $g_1$  and  $g_2$  on the interaction position in the detector, at most a 10-20% effect, and to the geometric efficiency calculation. Indeed, both  $\hat{\epsilon}(t_{\text{drift}})$  and  $\hat{\epsilon}_{S2}$  were calculated by disregarding the number of photons hitting the cathode in the area between PMTs. An upper bound to the size of this effect was evaluated by calculating the fraction of the cathode surface covered by the PMTs divided by the number of the top array PMTs and it amounts to  $\sim 10\%$ .

Rayleigh scattering was also not included in the efficiency calculation. An upper bound to the size of this effect could be obtained by re-calculating  $\hat{\epsilon}(t_{\text{drift}})$  and  $\hat{\epsilon}_{S2}$  with the inclusion in the toy Monte Carlo of the Rayleigh scattering probability for the UV-photons, with a scattering length of 90 cm [22], assuming that every scattered photon is lost. Eventually,  $\hat{\epsilon}_{S2}$  would decrease by  $\sim 30\%$ , whereas  $\hat{\epsilon}(t_{\text{drift}})$  by only  $\sim 15\%$ .

In the efficiency calculations we assumed no dependence on the angle of incidence on the cathode of the photoelectric efficiency, apart from the geometrical effects and that UV light attenuation in liquid argon is negligible.

The measured absorption length of TPB at 128 nm is about 400 nm [23]. Since this thickness is much smaller than the few microns of the TPB on the DS-50 cathode (see section 2), most photons are expected to give photoelectric effect in the TPB, and, therefore, QE is an estimate of the photoelectric quantum efficiency of the TPB, which is unmeasured so far. It should also be noted that this may not be compared directly with a measurement in vacuum. Indeed, it is known that there could be a modification of the effective work function of the TPB by the electron affinity of the liquid argon, as is expected for liquid xenon [8].

## 5. Bulk events

### 5.1. Event features

In addition to the S1-echo and S2-echo vertical and horizontal bands, in figure 6 there is also a continuum of events with no definite values of time differences of the SEC with either S1 or S2. Since these events follow in time the S2 signal, we call them *S2-bulk* events.

It is also possible to observe other events with no definite values of time difference of SEC with S1, by studying events with the

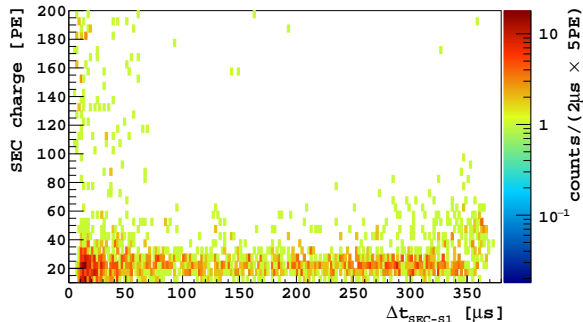


Figure 12: SEC charge vs. time difference  $\Delta t_{\text{SEC-S1}}$  distribution, in events with the time sequence S1-SEC-S2.

time sequence S1-SEC-S2. In figure 12, we show the SEC charge vs. time difference  $\Delta t_{\text{SEC-S1}}$  distribution. We notice that these events, apart from the first 30  $\mu\text{s}$ , are evenly distributed in time and with a SEC charge consistent with being single electrons. We call them *S1-bulk* events.

### 5.2. Event selection summary

The number of selected events after cuts,  $N_{ev}$ , in the different categories studied in the previous sections is shown in table 1. We used different  $\Delta t_{\text{S2-S1}}(\mu\text{s})$  cuts for S1-echo compared to S2-echo, to avoid spillover from S2-echo. The cut applied to S2-echo and S2-bulk is applied to be able to compare events where the limited data-acquisition time window does not affect the selection of S2-echo events. S1-echo events are much more rare than S2-echo events, by a factor of  $\sim 70$  (taking also into account a factor  $\sim 1.5$  in the ratio of the geometric efficiencies, i.e. the average value of  $\hat{\epsilon}(t_{\text{drift}})$ , see eq. (4), and  $\hat{\epsilon}_{\text{S2}}$ ).

### 5.3. Interpretation of bulk events

Understanding of the origin of S2-bulk and S1-bulk events is not straightforward. However, at least for the S2-bulk events, we can say that their larger number compared to the S1-bulk ones suggests a link with S2 photons, given the much larger

Table 1: Number of selected events after cuts,  $N_{ev}$ , in the different categories and with given  $\Delta t_{\text{S2-S1}}(\mu\text{s})$  cut.

Category	$\Delta t_{\text{S2-S1}}(\mu\text{s})$	$N_{ev}$
S2-echo	[5,45]	106964
S1-echo	[50,90]	2193
S2-bulk	[5,45]	8348
S1-bulk	[50,90]	184

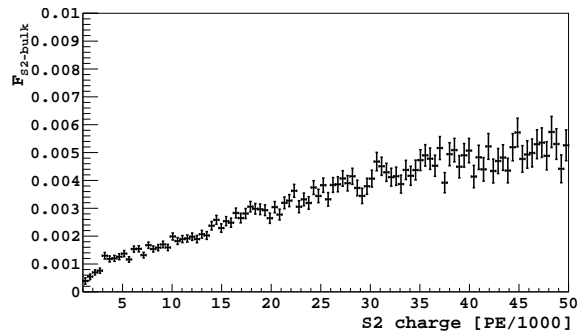


Figure 13: Fraction of S2-bulk events vs. S2 charge, with  $\Delta t_{\text{S2-S1}} > 50 \mu\text{s}$ .

S2 pulse charge compared to S1. However, while events with  $\Delta t_{\text{SEC-S1}} > 380 \mu\text{s}$  can only be caused by S2, for events with  $\Delta t_{\text{SEC-S1}} < 370 \mu\text{s}$  we do not know what fraction is due to S1 or S2. Another interesting observation for S2-bulk events is that also the fraction of S2-bulk events increases with S2 charge, as shown in figure 13.

A candidate explanation for the S2-bulk events is the photoionization by S2 photons (or S1 photons) of contaminants. One example is a contaminant which has previously captured an electron during a past event, such as for instance  $\text{O}_2^-$ , which has a relatively low ionization energy, namely below the 9.6 eV of liquid argon emission. The photoionization of neutral molecules such as  $\text{O}_2$  or  $\text{H}_2\text{O}$  is less likely since the first ionization energy is larger than 9.6 eV. Another possible explanation for the S2-bulk events is photoionization of TPB dissolved in the liquid.

To test the contaminant hypothesis, we analyzed a set of data taken in a time pe-

riod of five days in July 2015, when the getter was turned off for maintenance. As a matter of fact, during this period, we expect an increase of contaminants and, hence, an increase of photoionization in the bulk. Indeed, during the same time period, as described in a previous DS-50 paper [2], we observed a five-fold increase of isolated, i.e. far in time from a standard event, single electrons. However, with the data of this paper, we measure that the number of S2-bulk events increased only by  $\sim 35\%$ , with respect to the number of S2-echo events, indicating a somewhat different mechanism for the production of S2-bulk events from that of single isolated electrons. We disfavor the possible interpretation of the S2-bulk events as being due to recombination or molecule de-excitation since these mechanisms are not expected to yield electrons.

From the number of S2-bulk events, we derive the probability of photoelectric extraction from the liquid per unit length,  $PEP_{S2}$ , for  $5 \mu\text{s} < \Delta t_{S2-S1} < 45 \mu\text{s}$ , as

$$N_{S2\text{-bulk}} = \sum_r L(r) N_{S2}(r) \frac{\langle S2 \rangle}{g_2} PEP_{S2}, \quad (12)$$

where  $L(r)$  is the path length, inside a cylinder of diameter equal to that of the central PMT and height equal to the maximum TPC drift length, of an S2 photon generated at the radial distance  $r$ ,  $N_{S2}(r)$  the selected total number of events (two pulse and three pulse) vs  $r$ , and  $\langle S2 \rangle \sim 23,430$  PE.

Eventually, the measured  $PEP_{S2}$  is  $\sim 3 \times 10^{-6} e^-/\gamma_{UV}/\text{m}$ .

Due to the SEC pulse selection requirement of having the signal maximum in the central PMT, we tend to rule out the interpretation of S2-bulk events as photoelectric emissions from the lateral walls.

To fully understand the origin of these events, further experimental investigation is needed.

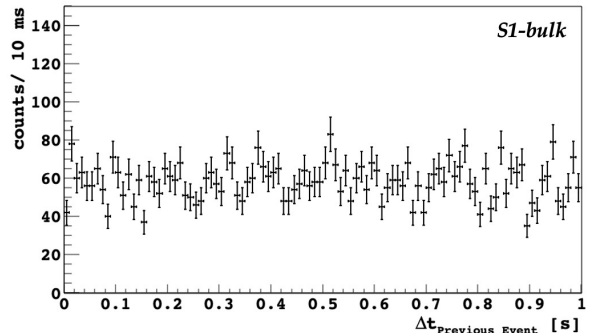


Figure 14: Distribution of the time difference of S1-bulk events with any previous event in a time window of 10 s, for  $SEC < 50$  PE. No specific selection on the previous events is applied.

As far as the S1-bulk events are concerned, there are two possible interpretations for the origin of the SECs: either they are due to S1 or they are remnants from previous events, e.g. electrons captured by some electronegative impurity and then released accidentally in the time window between S1 and S2. To test this hypothesis, we looked at a possible time correlation with the previous events. The time difference of S1-bulk events with any previous event in a time window of 10 s (out of which we only display 1 s), for  $SEC < 50$  PE, is shown in figure 14. No specific selection to the previous events is applied and the time of the events is defined here as the trigger time. According to a toy Monte Carlo simulation that we have performed, a time correlated component would show up as an exponential rise towards zero time. Therefore, from the experimental distribution, we can exclude, at present level of statistics, a correlated component with  $\tau \gtrsim 20$  ms.

A larger than average number of events per unit  $\Delta t_{SEC-S1}$ , and also with a higher SEC charge, is observed in figure 12 at small values of  $\Delta t_{SEC-S1}$ , below  $30 \mu\text{s}$ . A possible interpretation of these events is the photoionization of the extraction grid by S1 sig-

nals, as observed also with the LUX detector [8].

The ratio of number of S1-bulk to S2-bulk events also follows roughly the ratio between the S2 and S1 pulse charges, bearing in mind that we do not know what fraction of S2-bulk events is related to S1 and the inefficiency due to somewhat different selection cuts.

## 6. Discussion

We observed several categories of single isolated electrons in association with standard scintillation-ionization S1-S2 signals with the DS-50 LAr TPC. Since this is the first study in an argon detector, it is interesting to compare our results to the abundant literature available with xenon detectors. The LUX Collaboration [8] reports about four kinds of phenomena, three of which are also observed in DS-50: *photoionization electrons that are detected within hundreds of microseconds after the S1 and S2 pulses*, which are described in this paper, *delayed emission of individual electrons at the millisecond-to-second scale*, and *electron emission that appears independent of prior interactions*, that are briefly discussed in Ref. [2] and will be treated in more detail in a upcoming DS-50 publication. On the contrary, we do not observe in DS-50 *clustered electron emission that occurs within tens of milliseconds after S2*.

As far as photoionization electrons are concerned, their occurrence in xenon detectors has both similarities and differences with our findings.

We expect differences at least for the following reasons. The liquid to gas extraction efficiency with the electric fields used by the experiments is about 100% for argon, while it is only  $\sim 50\%$  for xenon [16], leading to potential electron trapping at the surface and, therefore, delayed electron emission. The

measured electron lifetime in DS-50 is much larger than both the lifetime measured by LUX (by more than a factor of 10) and the DS-50 maximum drift time (by a factor of 30). Therefore, electron capture by impurities during the drift is expected to be much less of a relevant issue in DS-50. This also implies that for DS-50 no efficiency correction is needed for S2 vs drift time. Another relevant difference is that the DS-50 cathode and anode planes are continuous planes, with the surface facing the active volume coated with ITO and TPB, whereas LUX uses metal grids and no wavelength shifting of the light.

S1-echo and S2-echo events are observed both with xenon detectors, e.g. LUX and XENON100 [10] and with DS-50. The quantum efficiency of TPB in DS-50 and of metal grids in LUX were measured. In both experiments they were calculated with both S1 and S2 photons and the results agreed in both cases within a factor of two.

In both LUX and DS-50 we observe photoionization events from the extraction grid, right below the gas-liquid interface.

Both S1-bulk and S2-bulk events are observed by both LUX and DS-50 Collaborations. Interesting considerations about the origin of S2-bulk events in LUX were obtained from the  $\Delta t_{S2-S1}$  distribution. Unfortunately, due to the limited time window of our data acquisition, we did not record on disk all S2-bulk events. Indeed, as shown in figure 6, all events above  $\Delta t_{SEC-S1} = 430 \mu s$  are cut out and, therefore, a  $\Delta t_{S2-S1}$  distribution (constant values of  $\Delta t_{S2-S1}$  are diagonal lines with unit slope in the figure) would be biased by the time acceptance cut. Nonetheless, it can be noticed that the S2-bulk event density is quite constant (even in linear scale) and, therefore, no significant dependence of the number of events on the interaction depth is observed.

S1-bulk and S2-bulk events are attributed

by LUX to the photoionization of impurities, more likely neutral molecules than negative ions, dissolved in liquid xenon. The hypothesis of photoionization in the liquid xenon was also suggested by the XENON-100 [10] Collaboration, which showed a correlation of the rate with the electron lifetime, and ZEPLIN-II Collaborations [9]. We also observed a correlation with the impurity concentration since we observed of a rate increase during a period of time with the getter switched off. However, our understanding of the origin of these events is only partial and inconclusive.

Both LUX and DS-50 measured the probability of photoelectric emission per unit length in the bulk. LUX measured  $(5-20)\times 10^{-5}e^{-}/\gamma_{UV}/m$  while DS-50 with S2-bulk events measured  $\sim 3\times 10^{-6}e^{-}/\gamma_{UV}/m$ . The smaller value found with DS-50 by more than a factor of 10, together with the much larger electron lifetime and the larger photon energy in DS-50 coherently hints toward a lower concentration of contaminants in DS-50. In both experiments, the identification of the impurity molecule was not possible and is left for future experimental work.

The S1-echo and S2-echo events observed with DS-50 are most probably going to be present also in DS-20k, given that the same wavelength shifter is going to be deposited on the cathode. Since the aspect ratio of the two TPCs is about the same, the number of expected echo events is going to scale with the ratio of background rates. For the S2-bulk events, there is going to be a factor of 5 more on top of the background rate factor, due to the larger drift length of DS-20k, were the level of contaminants is assumed to be the same.

## Acknowledgements

The DarkSide Collaboration offers its profound gratitude to the LNGS and its staff for their invaluable technical and logistical support. We also thank the Fermilab Particle Physics, Scientific, and Core Computing Divisions. Construction and operation of the DarkSide-50 detector was supported by the U.S. National Science Foundation (NSF) (Grants No. PHY-0919363, No. PHY-1004072, No. PHY-1004054, No. PHY-1242585, No. PHY-1314483, No. PHY-1314501, No. PHY-1314507, No. PHY-1352795, No. PHY-1622415, and associated collaborative grants No. PHY-1211308 and No. PHY-1455351), the Italian Istituto Nazionale di Fisica Nucleare, the U.S. Department of Energy (Contracts No. DE-FG02-91ER40671, No. DEAC02-07CH11359, and No. DE-AC05-76RL01830), the Polish NCN (Grant No. UMO-2014/15/B/ST2/02561) and the Foundation for Polish Science (Grant No. Team2016-2/17). We also acknowledge financial support from the French Institut National de Physique Nucléaire et de Physique des Particules (IN2P3) and the UnivEarthS LabEx program (Grants No. ANR-10-LABX-0023 and No. ANR-18-IDEX-0001), from the São Paulo Research Foundation (FAPESP) (Grant No. 2016/09084-0), from the Interdisciplinary Scientific and Educational School of Moscow University “Fundamental and Applied Space Research”, and from IRAP AstroCeNT funded by FNP from ERDF. Isotopes used in this research were supplied by the United States Department of Energy Office of Science by the Isotope Program in the Office of Nuclear Physics.

## References

- [1] J. Billard, E. Figueroa-Feliciano, and L. Strogari, *Phys. Rev. D* **89**, 023524 (2014).

- [2] P. Agnes et al. (The DarkSide Collaboration), *Phys. Rev. Lett.* **121**, 081307 (2018).
- [3] P. Agnes et al. (The DarkSide Collaboration), *Phys. Rev. Lett.* **121**, 111303 (2018).
- [4] C. E. Aalseth et al. (The DarkSide Collaboration), *Eur. Phys. J. Plus* **133**, 131 (2018).
- [5] P. Agnes et al., *Nucl. Instrum. Meth. A* **904**, 23 (2018).
- [6] M. G. Boulay and A. Hime, *Astropart. Phys.* **25**, 179 (2006).
- [7] A. Hitachi et al., *Phys. Rev. B* **27**, 5279 (1983).
- [8] D. S. Akerib et al., *Phys. Rev. D* **102**, 092004 (2020).
- [9] B. Edwards et al., *Astropart. Phys.* **30**, 54 (2008).
- [10] E. Aprile et al., *J. Phys. G* **41**, 035201 (2014).
- [11] D. Akimov et al., *Journal of Instrumentation* **11**, C03007 (2016).
- [12] P. Agnes et al. (The DarkSide Collaboration), *Phys. Rev. D* **98**, 102006 (2018).
- [13] D. Acosta-Kane et al., *Nucl. Inst. Meth. A* **587**, 46 (2008).
- [14] J. Xu et al., *Astropart. Phys.* **66**, 53 (2015).
- [15] A. Bondar et al., *Journal of Instrumentation* **4**, P09013 (2009).
- [16] E. M. Gushchin, A. A. Kruglov, and I. M. Obodovskil, *Zh.Eksp.Teor.Fi.* **82**, 1485 (1982).
- [17] P. Agnes et al., *Journal of Instrumentation* **12**, P12011 (2017).
- [18] P. Agnes et al. (The DarkSide Collaboration), *Phys. Lett. B* **743**, 456 (2015).
- [19] R. Acciarri et al., *Journal of Instrumentation* **5**, P05003 (2010).
- [20] P. Agnes et al., *Journal of Instrumentation* **12**, P10015 (2017).
- [21] P. Agnes et al., *Eur. Phys. J. C* **81**, 1014 (2021).
- [22] M. Babicz et al., *Journal of Instrumentation* **15**, P09009 (2020).
- [23] C. Benson, G. Orebi Gann, and V. Gehman, *Eur. Phys. J. C* **78**, 329 (2018).